Case Study: Oso, Washington, Landslide of March 22, 2014—Material Properties and Failure Mechanism

Ahmed Baghdady

Journal of Geotechnical and Geoenvironmental Engineering

Case Study: Oso, Washington, Landslide of March 22, 2014—Material Properties and Failure Mechanism

Timothy D. Stark, F.ASCE[1]; Ahmed K. Baghdady, S.M.ASCE[2]; Oldrich Hungr, M.ASCE[3]; and Jordan Aaron, S.M.ASCE[4]

Abstract: This paper describes investigation, testing, analysis, and slope history used to determine the two-phase failure mechanism involved in the 2014 landslide near Oso, Washington. The first phase involves a slide mass located above the frequent landslides in the lower portion of the slope and extends to near the slope crest. This slide mass had a large potential energy, which moved downslope, and pushed the water-filled colluvium that had accumulated along the slope toe across the valley, resulting in it flowing almost 1.5 km. Evacuation of the Phase I slide mass left the upper portion of the slope unbuttressed and oversteepened, causing a second landslide (Phase II) but it primarily remained on the source slope because the back edge of the Phase I slide mass prevented further movement and the dense and unsaturated upper soils did not undergo a significant strength loss like the water-filled colluvium. **DOI: 10.1061/(ASCE)GT.1943-5606.0001615.**

Author keywords: Landslide; Failure mechanism; Slope stability analysis; Light detection and ranging (LiDAR); Shear strength; Kinematics; Flow slide; Liquefaction.

Introduction

On March 22, 2014, a large and fast-moving landslide destroyed the Steelhead Haven Community near Oso, Washington, along the North Fork of the Stillaguamish River in Snohomish County, Washington. This landslide is also referred to as the SR530 Landslide because the flowslide debris buried Washington State Route 530 (SR530) that connects Oso and Darrington, Washington, and some Oso residents prefer not to name the landslide after their community. For consistency with prior publications (Keaton et al. 2014; Iverson et al. 2016; Wartman et al. 2016), the event is called the Oso landslide herein. This landslide is considered the deadliest in the history of the continental United States with 43 fatalities (Wartman et al. 2016). The entire landslide involved approximately 8.3 million m^3 of glacial deposits and water-filled colluvium from prior landslides present along the slope toe. The colluvium-derived flowslide traveled more than 1.5 km to its distal edge on the south side of SR530. During various site visits (May 22–24, 2014, February 28, 2015, and April 16, 2015), the authors examined landslide features and exposed geology, obtained soil samples for laboratory testing to estimate engineering properties, reviewed aerial photographs, and conducted stability analyses to assess the impact of changes in slope geometry with time. This paper summarizes the material properties measured during this investigation and the postulated two-phase failure mechanism for the 2014 landslide.

Regional Physiography and Geology

The crest of the Oso landslide slope is located at elevation of approximately 270 m (880 ft) on the north side of the west-trending valley of the Stillaguamish River, which is at elevation of approximately 75 m (246 ft). This corresponds to a slope height of approximately 200 m (650 ft). The width of the Stillaguamish River Valley floor at this location varies from 2.0 km to more than 6.0 km. This slope is part of a large glacial terrace deposit that developed after the last advance of continental glacial ice sheets into the Puget Sound. The 2014 landslide occurred at a relatively narrow reach of the river, where it flows north and then west along the slope toe. The river erosion, especially at the eastern end, has caused a number of landslides in the lower portion of the slope including landslides in 1937, 1951, 1952, 1967, 1988, and 2006, (see 2006 landslide in Fig. 1). The 2014 landslide did not involve bedrock but the bedrock in the immediate landslide area consists of Jurassic metasedimentary, metavolcanic, and ultramafic rocks in the western portion of the valley and Tertiary sedimentary and volcanic rocks in the eastern portion (Dragovich et al. 2003; Keaton et al. 2014). Quaternary-age surficial deposits overlie the bedrock and include a series of deep glacial soil deposits, which are discussed subsequently.

Subsurface Conditions

Knowledge of the pre-2014 landslide subsurface conditions is important for understanding the failure mechanism because a

[1]Professor, Dept. of Civil and Environmental Engineering, Univ. of Illinois at Urbana-Champaign, 205 N. Mathews Ave., Urbana, IL 61801 (corresponding author). E-mail: tstark@illinois.edu

[2]Ph.D. Student, Dept. of Civil and Environmental Engineering, Univ. of Illinois at Urbana-Champaign, 205 N. Mathews Ave., Urbana, IL 61801. E-mail: baghdad2@illinois.edu

[3]Professor, Dept. of Earth and Ocean Sciences, Univ. of British Columbia, Vancouver, BC, Canada V6T 1Z4. E-mail: ohungr@eos.ubc.ca

[4]Ph.D. Student, Dept. of Earth and Ocean Sciences, Univ. of British Columbia, Vancouver, BC, Canada V6T 1Z4. E-mail: Jordan_aaron49@hotmail.com

Note. This manuscript was submitted on January 19, 2016; approved on July 18, 2016; published online on January 18, 2017. Discussion period open until June 18, 2017; separate discussions must be submitted for individual papers. This paper is part of the ***Journal of Geotechnical and Geoenvironmental Engineering***, © ASCE, ISSN 1090-0241.

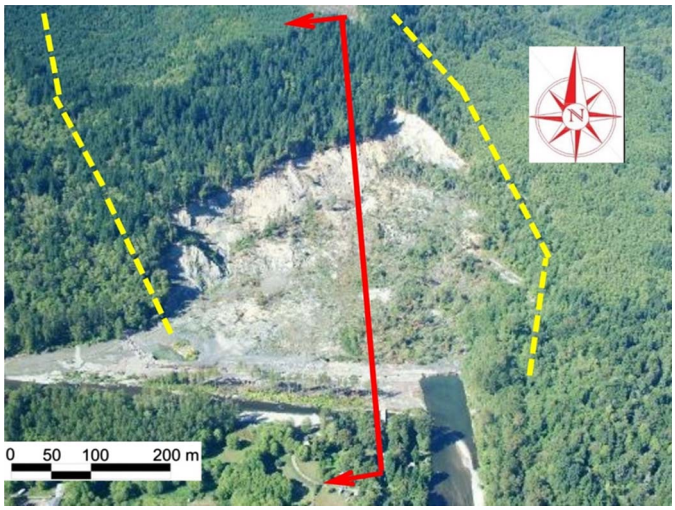

Fig. 1. Aerial view of 2006 landslide, location of cross section in Fig. 2 (solid line), and outline of sides of 2014 landslide (dashed lines) (image courtesy of Rupert G. Tart)

comparison of the initial and final locations of the various glacial soil deposits aids the understanding of landslide initiation, movement, and runout. Based on the exposed landslide head scarp, hand and shovel excavations during various site visits, geologic maps, borings before (Shannon 1952) and after the landslide (Badger 2015), and soil samples collected and tested herein, the subsurface profile prior to the 2014 landslide is shown in Fig. 2 and located at the cross section location in Fig. 1. This subsurface profile consists of (from top to bottom):

1. Recessional outwash: Tan to light brown unsaturated cohesionless fluvial deposits, medium-dense to dense fine to coarse sands with cross beddings. The thickness of this outwash is approximately 40 m (130 ft) from elevation 270 to 230 m (886 to 755 ft). The top of this deposit is referred to locally as the Whitman Bench or Upper Plateau (Fig. 2).
2. Glacial till: Light gray unsaturated stiff to very stiff, consolidated, and unsorted mixtures of clay, silt, sand, and gravels with scattered cobbles and boulders. The thickness of this layer is approximately 21 m (70 ft) from elevation 230 to 207 m (755 to 680 ft).
3. Advanced outwash: Tan to light brown unsaturated fluvial medium-dense coarse sand and sandy gravel with localized clay and silt interbeds. The advanced outwash thickness is approximately 30 m (100 ft) from elevation 207 to 177 m (680 to 580 ft).
4. Advanced glaciolacustrine: Light to dark gray, medium stiff to stiff, unsaturated to saturated with horizontally laminated low- to high-plasticity clays and silts with occasional fine sands laminae. The lower thickness of this layer is approximately 82 m (270 ft), from elevation 177 to 95 m (580 to 310 ft), and was also involved in most, if not all, of the prior landslides caused by river erosion of the deposit along the slope toe. The unsaturated condition of the Advanced Glacio-Lacustrine deposit is evident in surficial exposures and in available borings. Higher degrees of saturation may exist further behind the eroded valley scarp.
5. Sands and gravels: Well-sorted fine- to medium-grained sands and gravel with possible artesian pressures.
6. Fluvial deposits and alluvium: Oxidized deposits of loose saturated sands and silts forming the river floodplain, mixed with debris from prior landslides exposed near the base of the slope; it is youngest deposit and not part of the stratigraphic sequence.

Material Properties

This section briefly presents the material properties used to (1) assess the failure mechanism below, (2) perform two-dimensional (2D) limit equilibrium stability analyses to estimate probable groundwater levels for the ancient (Fig. 2), 1967, and 2006 landslides in the lower portion of the slope, and (3) identify likely failure surfaces for the Phase I and Phase II landslide masses discussed subsequently. Fifteen hand- and shovel-excavated samples were obtained during various site visits and used in laboratory testing at the University of Illinois. Four additional samples were provided by Snohomish County for testing for a total of 19. Because of the unsaturated and dense nature of the outwash sands and glacial till in the upper portion of the slope, the laboratory testing focused on the

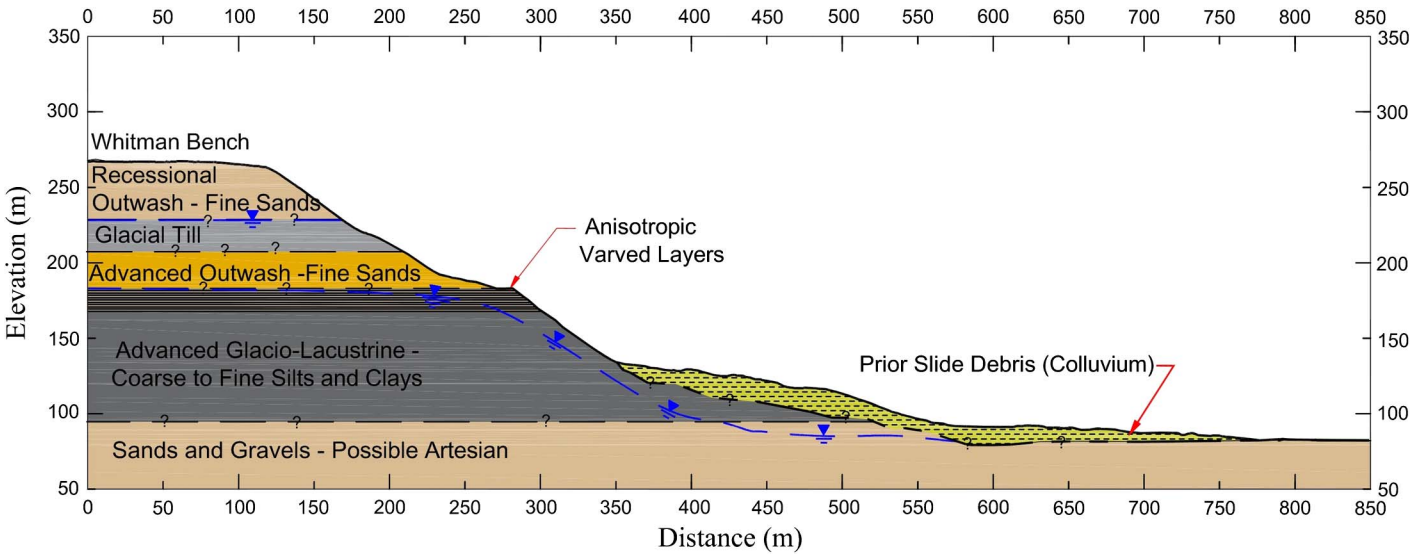

Fig. 2. Slope cross section at location in Fig. 1 prior to 2014 landslide with phreatic surfaces inferred from inverse stability analyses except where observed in borings from the Whitman Bench

J. Geotech. Geoenviron. Eng., 2017, 143(5): -1--1

advanced glaciolacustrine clay deposit in the lower portion of the slope.

Sensitivity of the advanced glacio-lacustrine clay deposit was investigated to determine if sensitivity contributed to the observed strength loss and runout distance of the slide mass. Laboratory vane shear [ASTM D4648-16 (ASTM 2016)] and pocket penetrometer [ASTM WK27337 (ASTM 2015)] tests were used to estimate soil sensitivity for eight samples of the advanced glaciolacustrine clays including the four samples provided by Snohomish County. The peak undrained vane strength and the strength after 10 revolutions of the vane [ASTM D4648-16 (ASTM 2016)] were divided to estimate sensitivity. The peak undrained strength also was measured using a pocket penetrometer [ASTM WK27337 (ASTM 2015)] on intact samples and the remolded strength was measured using a reconstituted specimen obtained from the area where the peak undrained strength was measured.

The advanced glaciolacustrine clay deposits exhibited sensitivities of 1.4–3.3, respectively. Based on Peck et al. (1974), these sensitivity values correspond to normal sensitivity (1–4), where a sensitivity greater than 4 is considered sensitive and greater than 8 is extra sensitive. Therefore, the intact and undisturbed advanced glaciolacustrine clay deposit is not sensitive and did not undergo a significant strength loss, which helped confirm that a deep-seated failure surface did not develop and result in the observed runout as conceptualized by Keaton et al. (2014). A deep-seated circular failure surface as proposed by Keaton et al. (2014) also would not experience such mobility because as it moves or rotates, the driving forces are reduced.

Another indicator of potential strength loss in the advanced glaciolacustrine clay is liquidity index (LI). In general, a LI value of unity (1) indicates the water content is at the liquid limit (LL) so there is limited potential for additional moisture increase and with some disturbance the material could behave like a fluid. For example, quick clay landslides in Norway and Canada have occurred in low-plasticity materials that have a LI greater than unity. Holtz et al. (2011) present a relationship between LI and sensitivity with LI ranging from 1 to 4 and soil sensitivity ranging from 2 to 1,000 for these values of LI.

Conversely, a LI of 0 indicates the water content is at the plastic limit (PL) and the soil is not likely to undergo a significant strength loss if disturbed. Table 1 shows the measured values of in situ water content, LL, PL [ASTM D4318-10 (ASTM 2010a)], and LI for the advanced glaciolacustrine clay deposit. The values of LI range from 0.2 to 0.3 for 12 samples, also indicate the advanced glaciolacustrine clay deposit is not likely to undergo a significant strength loss if disturbed. This corroborates the previous laboratory vane shear and pocket penetrometer data and confirms that the undisturbed, overconsolidated glaciolacustrine clays are not sensitive and susceptible to significant strength loss like quick clays. The samples were obtained during various site visits by excavating with a shovel and/or hand trowel so the samples are a better representative of the natural water content than surficial soils and thus not significantly drier or wetter than weather conditions at the time of the 2014 landslide.

Three oedometer and consolidation tests [ASTM D2435-11 (2011)] were also performed on the larger block samples of the advanced glaciolacustrine clay deposit because they were viewed as less disturbed than the smaller blocks. All block samples were obtained using shovels or hand trowels and sealed in two resealable plastic bags to preserve moisture during various site visits and transport. These tests confirm the heavily overconsolidated nature of the advanced glaciolacustrine clays with the maximum preconsolidation pressure and overconsolidation ratio (OCR) being measured to be 1,628 kPa (34,000 psf) and 8, respectively. The range of OCR for all of the samples tested is 4–8.

Fully softened (FSS) and residual shear strengths of the advanced glaciolacustrine clay deposit were measured using a torsional ring shear device in accordance with ASTM D7608 (ASTM 2010b) and ASTM D6467 (ASTM 2013), respectively. As expected, the shear strength envelopes are stress dependent (Stark and Hussain 2013) so the friction angles in Table 1 represent the secant friction angles for the normal effective stresses used in the testing. The FSS and residual stress-dependent strength envelopes shown in Fig. 3 were used directly in the 2D limit equilibrium stability analyses discussed subsequently. The fully softened and residual friction angles in Table 1 are in agreement with empirical correlations in Stark and Hussain (2013) and Gamez and Stark (2014) for the measured liquid limit and clay-size fraction values in Table 1.

As a result of the measured sensitivities and shear strengths, the failure mechanism investigation started focusing on the water-filled colluvium along the slope toe as the material that could have undergone a large undrained strength loss and contributed to the 1.5-km runout instead of the intact and heavily overconsolidated advanced glaciolacustrine clays.

Landslide History

The 2014 landslide occurred in a slope with a history of prior landslides. Modern accounts of landslides in the lower portion of the slope date back to 1932 (Thorsen 1969). More recent high-resolution topographic relief images generated by light detection and ranging (LiDAR) show many large prehistoric landslides including one at the location of the 2014 landslide have occurred in this valley. The documented history of landsliding at this site reveals two types of event: (1) large prehistoric landslides that involve the upper glacial terrace deposits, i.e., the Whitman Bench (Figs. 2 and 4), which are similar to the 2014 landslide, and (2) smaller landslides in the lower portion of the slope primarily caused by river erosion. All of the landslides between 1937 and 2006 are small and occurred in the lower portion of the slope. Landslides involving the Whitman Bench exhibit significantly greater

Table 1. Summary of Index Property and Shear Strength Testing for Upper and Lower Glaciolacustrine Deposits

Engineering property	Low-plasticity advanced glaciolacustrine	High-plasticity advanced glaciolacustrine
Liquid limit [ASTM D4318-10 (ASTM 2010a)]	34–38 (average = 36)	52–60 (average = 55)
Plastic limit	21–24 (average = 22)	25–29 (average = 26)
In situ water content (%)	23–28 (average = 25)	32–37 (average = 34)
Liquidity index	0.2–0.25	0.27–0.3
Sensitivity	1.4–2.2	2.8–3.3
Clay-size fraction (% <0.002 mm) [ASTM D422-07 (ASTM 2007)]	31–36%	51–56%
Fully softened friction angle (effective normal stresses of 12, 50, 100, and 400 kPa)	25–34°	21–32°
Residual friction angle (effective normal stresses of 50, 100, 400, and 700 kPa)	20–27°	12–19°

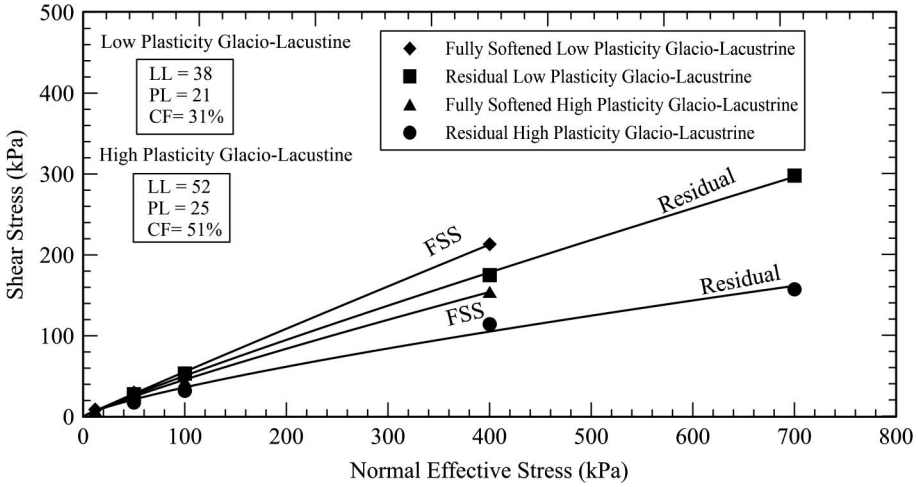

Fig. 3. Fully softened and residual strength envelopes for advanced glaciolacustrine clay deposits

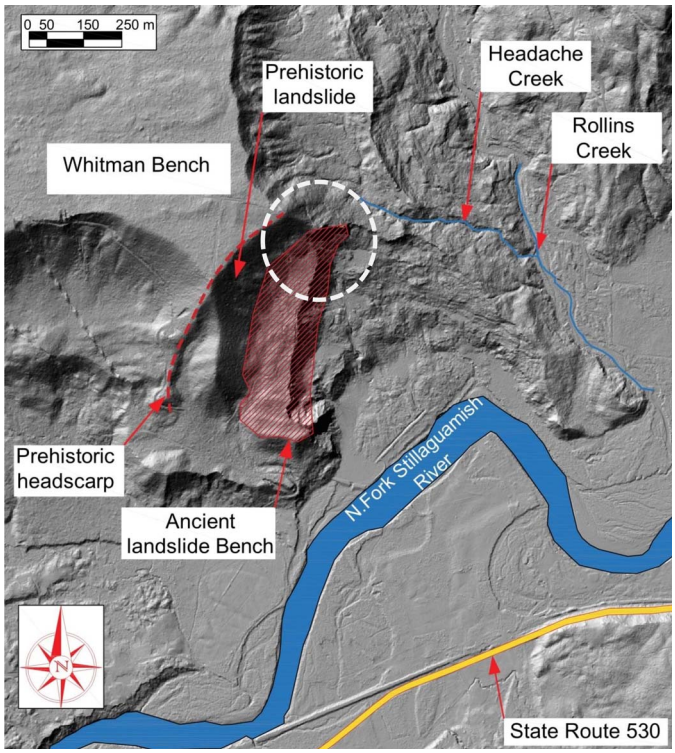

Fig. 4. 2013 LiDAR-derived topography showing the Oso, Washington, landslide in context with the Ancient Landslide Bench (base courtesy of Puget Sound Lidar Consortium)

runout because of the greater elevation and potential energy of the source material than the low-elevation landslides.

The occurrence of a large prehistoric landslide at the location of the 2014 landslide is important because it created the Ancient Landslide Bench shown in Fig. 4 that supported and protected the Whitman Bench from landslides in the lower portion of the slope primarily caused by river toe erosion and precipitation. Based on the geometry of neighboring high-elevation landslides also shown in Fig. 4, it is anticipated that the ancient landslide at this location occurred through the weak varved lacustrine layers in the upper portion of the advanced glaciolacustrine deposit and evacuated some of the overlying Whitman Bench. After this landslide, a bench or ledge was created that supported the overlying Whitman Bench slope (Fig. 5) and protected the Whitman Bench from oversteepening by landslides in the lower portion of the slope primarily caused by river toe erosion until after 2006.

The ancient slide mass traveled down the slope and across the Stillaguamish River, where it was eroded over geologic time (Fig. 5). This is easy to visualize because the ancient slide mass consisted primarily of two unsaturated sandy outwash deposits that are easily eroded by the river as witnessed after the 2014 landslide. During a site visit only 2 months after the 2014 landslide, a significant amount of these sandy outwash deposits had already been eroded by the Stillaguamish River. This explains the lack of a significant portion of the ancient slide mass (Fig. 5) being present on the valley floor prior to the 2006 and 2014 landslides.

Aerial photographs of the 1937, 1951, 1952, 1967, 1988, and 2006 landslides assembled by the Seattle Times (2016), Kim et al. (2015), and Sun et al. (2015) show only the lower portion of the slope was involved and these landslides involved only the advanced glaciolacustrine clay deposit. These landslides in the lower portion of the slope removed some of the Ancient Landslide Bench but there was still sufficient width of the bench to support the overlying Whitman Bench until after the 2006 landslide. The slide masses from these lower elevation landslides remained on the lower slope or advanced only 85 m (280 ft) in the 1947 slide, 200 m (656 ft) in the 1967 slide, and 250 m (820 ft) in the 2006 slide from the slope toe because of their low elevation, low potenial energy, and lack of significant strength loss. Nevertheless, in each of these low-elevation landslides the slide mass would move the active river channel to the south away from the slope toe. The river would then start eroding the prior landslide debris to the north until it was again undermining the advanced glaciolacustrine clays. Based on the dates of prior landslides and aerial photographs, it took approximately 35–40 years to erode enough landslide debris and colluvium to initiate another landslide in the lower portion of the slope. Each of these landslides would remove some of the Ancient Landslide Bench, especially on the eastern end where the river flowed directly into the slope (Fig. 4). This timing of 35–40 years is important because only 8 years elapsed between the 2006 landslide and the large 2014 landslide, not 35–40 years, so a different failure mechanism was involved in 2014.

Fig. 6 presents the slope cross section shown in Fig. 1 and the difference in slope topography from the 2003 and 2013 LiDAR images. Using the difference in topography from 2003 and 2013,

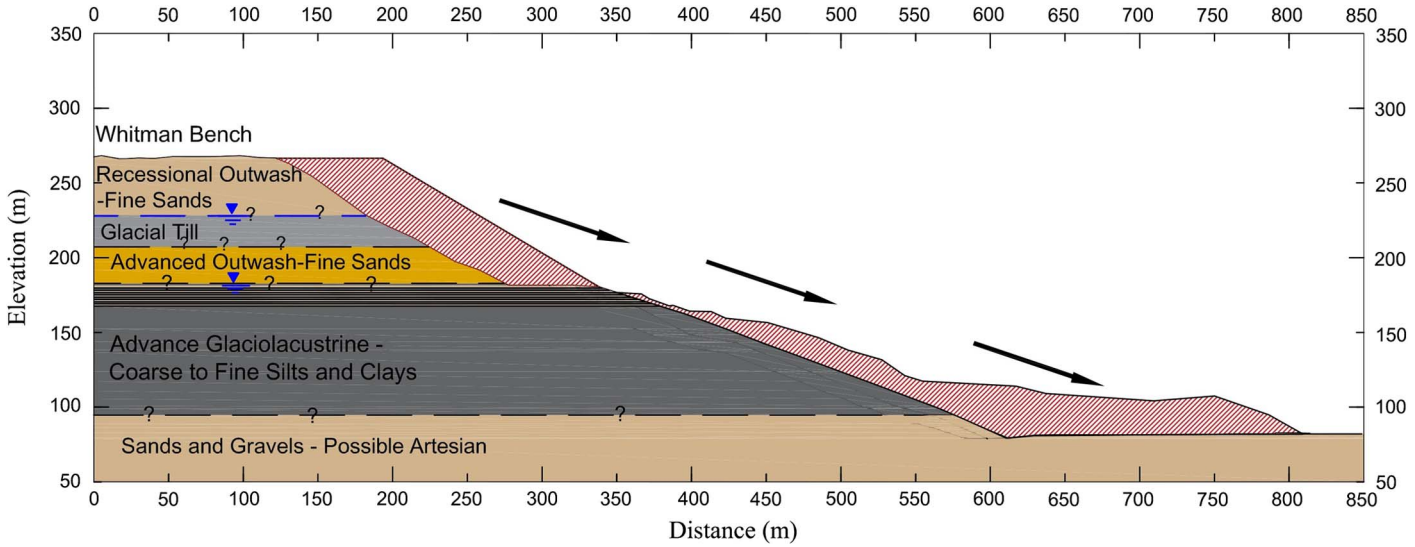

Fig. 5. Hypothesis of prehistoric landslide showing depletion zone, slide mass in valley, and landslide bench near the top of the upper glaciolacustrine deposit based on LiDAR image in Fig. 4 at cross section location shown in Fig. 1

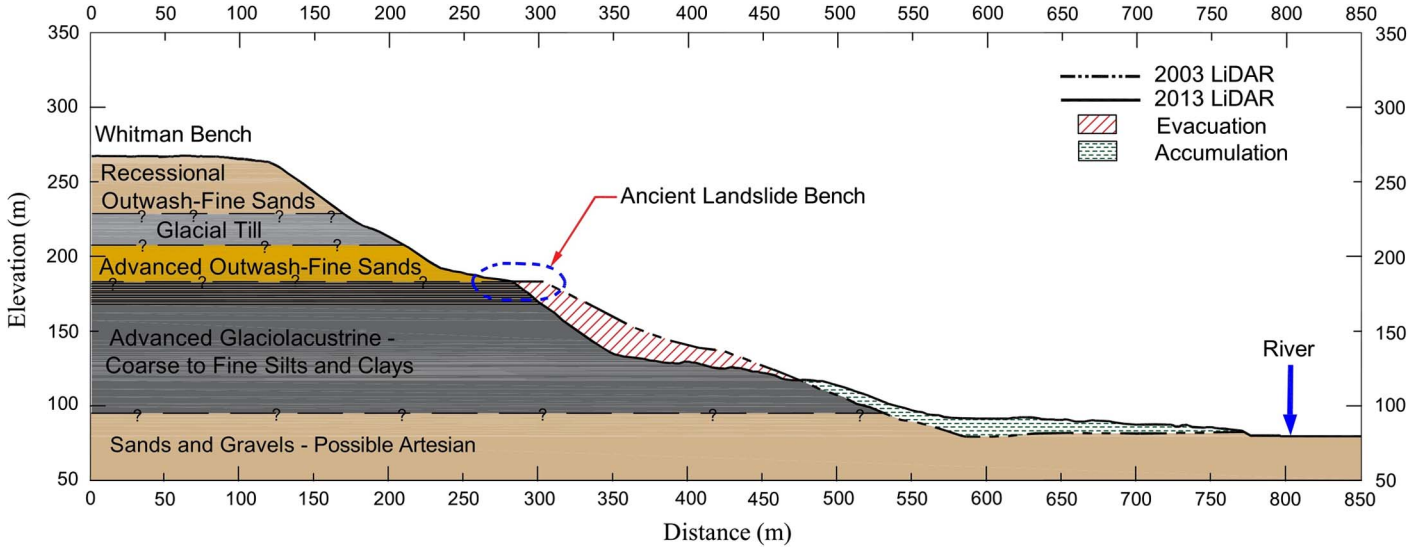

Fig. 6. Differences in surface topography between 2003 and 2013 and locations of the depletion and accumulation zones for the 2006 landslide at the cross-section location shown in Fig. 1

the depletion and accumulation zones for the 2006 landslide were determined and are shown in Fig. 6. These zones show that the source of the 2006 landslide mass is the advanced glaciolacustrine deposit and the resulting colluvium moved the river to the southern extent of the accumulation zone. This is important for concluding that the Stillaguamish River erosion did not contribute to the 2014 landslide because the river was pushed significantly south (horizontal distance of approximately 800 m in Fig. 6) of the Ancient Landslide Bench (horizontal distance of approximately 300 m in Fig. 6) after the 2006 landslide. More importantly, the colluvium from the 2006 landslide added to the existing colluvium that had accumulated along the slope toe.

Fig. 6 also shows that the upper portion of the depletion zone removed approximately 21 m (70 ft) of the Ancient Landslide Bench at this cross section location, i.e., the eastern end of the bench (Badger 2015). Fig. 4 shows that most of the eastern side of the Ancient Landslide Bench was removed by prior landslides in the lower portion of the slope (see dashed white circle in Fig. 4) and provided little support to the overlying Whitman Bench in 2014, compared with the wide bench at the western end. The eastern portion of the Ancient Landslide Bench was significantly narrower than the western end because the river flows almost directly north into the slope at the eastern end and then runs parallel to the slope toe toward the west, causing more erosion and landslides on the eastern side than the western side. For example, Fig. 7 shows the river cutting deeper into the slope on the eastern end than the western end in 1947, 1951, 1965, and 2006 based on the river location obtained from aerial photographs in these years. Fig. 8 shows the northward progression of the scarps into the Ancient Landslide Bench on the eastern end from 1967 to 2013, which left the Whitman Bench slope marginally supported after the 2006 landslide.

Fig. 7 also shows the changes in the Stillaguamish River channel with time and shows that the river channel was pushed south after

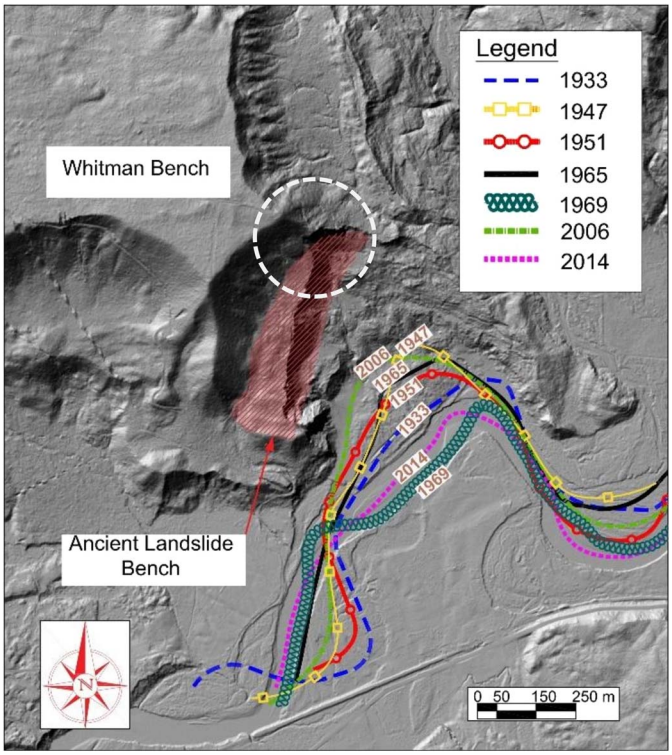

Fig. 7. Changes in Stillaguamish River channel between 1933 and 2014 due to prior landslides in the lower portion of the slope shown on 2013 LiDAR-derived topography (base courtesy of Puget Sound Lidar Consortium)

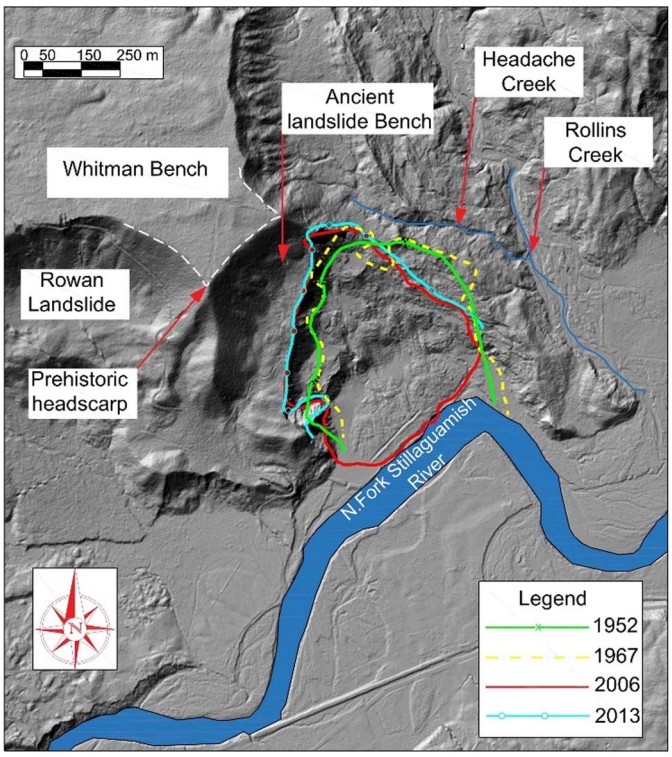

Fig. 8. Location of historic landslide scarps from 1952 to 2013 shown on 2013 LiDAR-derived topography (base courtesy of Puget Sound Lidar Consortium)

the 1967 and 2006 landslides. Stability analyses of the 1967 and 2006 slopes show the factor of safety decreased from approximately 1.18 to 1.02 due to the toe erosion over these 39 years. Therefore, the lower portion of the slope was marginally stable even after river erosion induced a landslide because the factor of safety is less than 1.2. Table 2 presents the input parameters used for the limit equilibrium stability analyses reported herein.

2014 Landslide

The 2014 landslide is significantly different than the 1937, 1951, 1952, 1967, 1988, and 2006 landslides in the following four main aspects:

1. River erosion did not play a significant role because the river channel had been pushed significantly south of the slope by the 2006 landslide (Fig. 6);
2. The 2014 landslide occurred only 8 years after the 2006 landslide, not 35–40 years;
3. Slide mobility was much greater, resulting in the slide mass traveling more than 1.5 km in comparison to 85 m (280 ft), 200 m (656 ft), and 250 m (820 ft) in the 1947, 1967, and 2006 landslides, respectively (Iverson et al. 2016); and
4. The 2014 slide mass is much larger than the 1937, 1951, 1952, 1967, 1988, and 2006 slide masses.

As a result, a different failure mechanism than river toe erosion had to initiate the 2014 landslide. The first factor considered for the 2014 landslide is precipitation. The 2014 landslide occurred during a dry sunny morning after a period of unusually intense rainfall. Nearby precipitation gauges with 86 years of data indicate the rainfall during the month preceding the landslide was significantly greater than average (Keaton et al. 2014). In particular, these data show the 45-day period before the landslide was wetter than 98% of the same 45-day period in the 86-year historical record (Iverson et al. 2016). Cao et al. (2014) and Henn et al. (2015) show the cumulative precipitation for the 21 days prior to the March 22, 2014, landslide corresponds to a return period of approximately 97 years, making the 21 days prior to the landslide the wettest [403 mm (15.8 in.)] on record at the Darrington, Washington, rain gauge. It is anticipated this intense rainfall, higher groundwater, and increased runoff along the eastern side of the 2014 landslide mass triggered a landslide that removed the small remaining portion of the Ancient Landslide Bench on the eastern end (see dashed circle in Fig. 7), and undermined the Whitman Bench slope as discussed subsequently. This resulted in the initiation of the two-phase failure mechanism described subsequently.

In summary, the rainfall during the fall 2013 and winter 2014 was below average to average, but the rainfall from March 1 to 22, 2014, corresponds to a 97-year return period and is the wettest time period in the 86 years of historical data. Even with a record rainfall in March 2014, the Oso landslide is the only large landslide in the valley and region so this site had a unique feature, i.e., an oversteepened and/or undermined Ancient Landslide Bench on the eastern end. LiDAR images show no other ancient landslide bench in this area was oversteepened and/or undermined to the extent of the bench shown in Fig. 7.

Phase I of Failure Mechanism: Initial Slide Mass

Based on inverse 2D limit equilibrium stability analyses using the software packages *SLIDE* and *SLOPE/W* and the soil properties in Table 2, Fig. 9 shows the probable failure surface for the initial instability that triggered the first phase (Phase I) of the 2014 two-phase failure mechanism. This instability initiated in the eastern portion of the Ancient Landslide Bench slope (Fig. 7) where the

Table 2. Input Parameters for Limit Equilibrium Slope Stability Analyses

Geologic deposit	Total and saturated unit weights (kN/m^3)	Effective stress friction angle or range of friction angle for stress-dependent strength envelope		
		Estimated peak (degrees)	Measured fully softened (degrees)	Measured residual (degrees)
Recessional outwash	20.0	28	—	—
Glacial till	20.0	35	—	—
Advanced outwash	19.0	30	—	—
Low-plasticity advanced glaciolacustrine	20.0	—	25–34	20–27
High-plasticity advanced glaciolacustrine	20.0	—	21–32	12–19
Sands and gravels	19.0	35	—	—
Prior slide debris (colluvium)	16.5	—	21–32	12–19

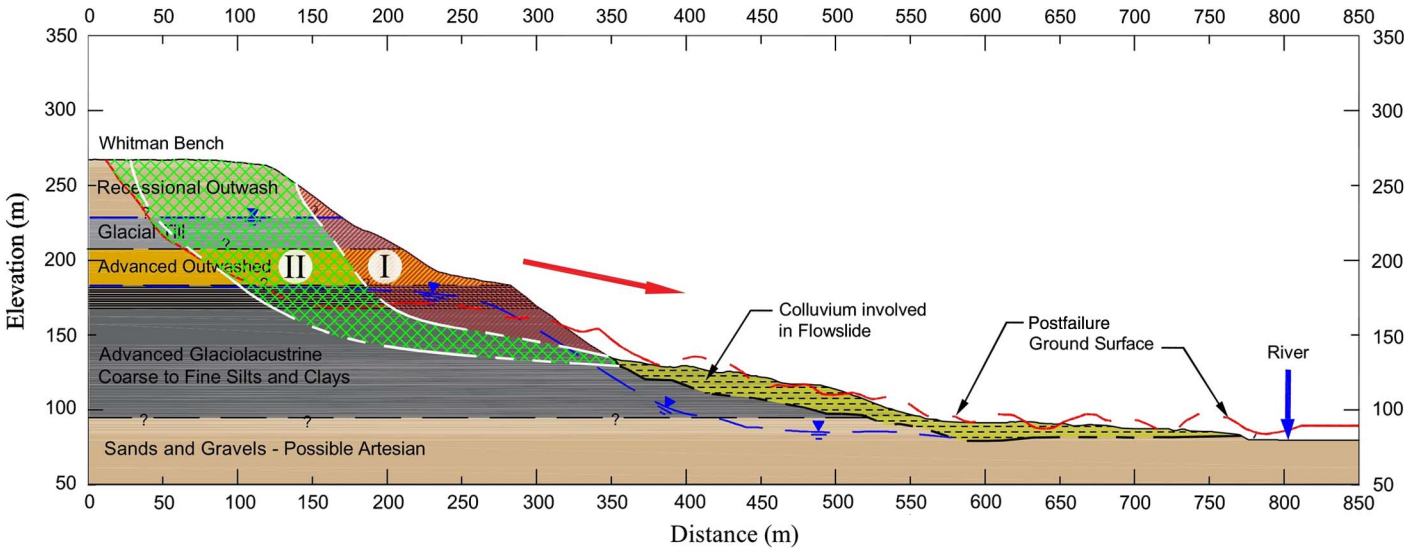

Fig. 9. Two-phase failure mechanism prior to 2014 landslide with the Phase 1 failure surface based on field observations and inverse slope stability analyses at cross section location shown in Fig. 1

bench had been oversteepened by prior sliding in the lower portion of the slope. The failure surface in Fig. 9 is based on field observations and inverse stability analyses that yielded a factor of safety of approximately unity for a variety of compound failure surfaces and piezometric levels estimated from the inverse analysis of the 2006 landslide.

Compound slip surfaces were primarily considered because of the observed internal distortion of the slide volume during each of the two phases and the differing soil types in the upper portion of the slope, i.e., outwash sands, glacial till, and varved silts and clays in the advanced glaciolacustrine deposit that contain weak horizontal layers as discussed previously. However, a circular search also was conducted, which confirmed the critical failure surface is a compound slip surface. Circular (Keaton et al. 2014) and log spiral (Iverson et al. 2016) failure surfaces are relevant for homogenous and isotropic materials, such as soft clays, not the variable, anisotropic, and possibly presheared glacial terrace deposits present in this slope.

Colluvial Flowslide of Phase I

The important aspect of the Phase I initial slide mass is that it quickly impacted the disturbed, water-filled, softened, and blocky colluvium along the lower portion of the slope as it moved downslope. At the western end of the slope, a 0.9–1.2 km^2 (15–20 acres) sedimentation pond with a depth of 4.6 m (15 ft) had been constructed in the colluvium after the 2006 landslide to reduce the amount of sediment entering the river due to precipitation, emergent stream(s) and seepage from the slope, and river flooding. Therefore, the colluvium had an abundance of water between the blocks of overconsolidated clay and within the loose matrix of disturbed soil filling these interstices. Many of the intact blocks were likely also at or near saturation. All of this helped produce a fluid or liquefied behavior after being impacted by the Phase I slide mass, which is described subsequently. The Phase I initial slide mass was moving rapidly downslope in its descent of approximately 150 m (490 ft) when it impacted the colluvium causing an extreme undrained strength loss, which allowed the colluvium to flow across the river and valley. With the large and rapid impact force from the Phase I initial slide mass, the blocky, softened, and water-filled colluvium disintegrated into a fluid condition with the soil particles becoming suspended in a fluid matrix causing a flowslide using the classifications in Hungr et al. (2014). The fluid colluvium then flowed quickly across the valley like a flowslide ahead of the Phase I initial slide mass. Without the large and rapid push of the Phase I initial slide mass, the colluvium would not have undergone this large undrained strength loss because similar colluvium was present prior to the low-elevation landslides in 1937, 1951, 1952, 1967, 1988, and 2006 and these slide masses did not flow across the valley. Therefore, the large-scale and significant undrained strength loss of the colluvial mass appears to be contingent on a sufficiently massive and energetic impulse from above, which

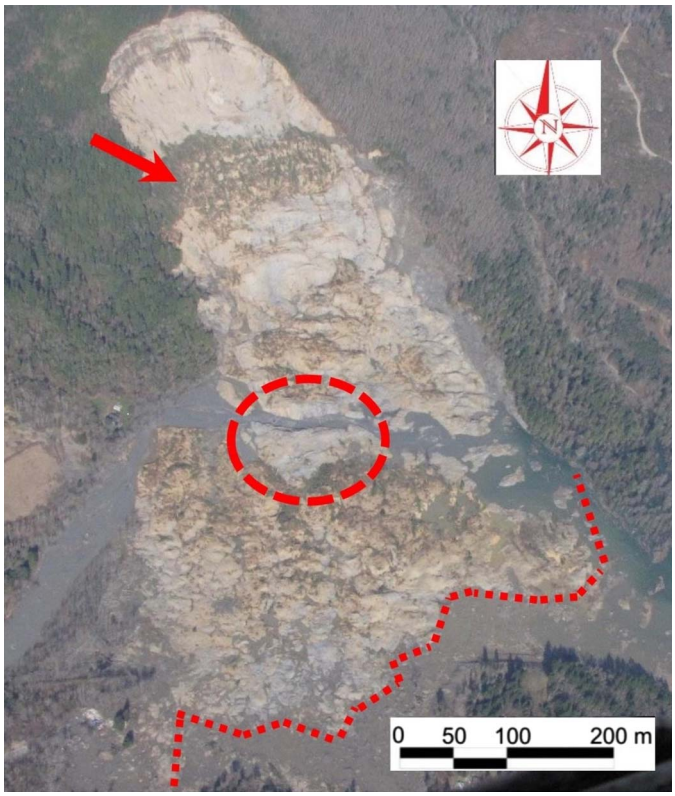

Fig. 10. Aerial view of extent of sand (dashed line) pushing and overriding fluidized colluvium from the slope toe, a new landslide bench (arrow), and the Phase II slide mass overriding back end of Phase I slide mass (dashed circle) (image courtesy of Rupert G. Tart)

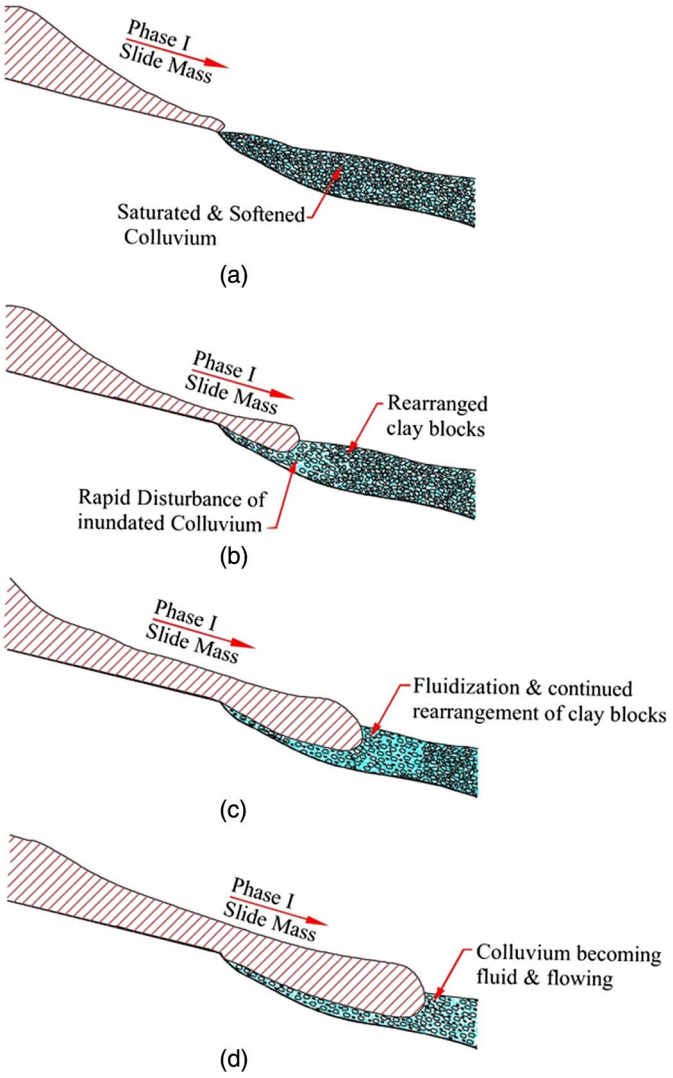

Fig. 11. Schematic of Phase I slide mass rapidly moving downslope and initiating the colluvial flow slide: (a) rapid upslope slide; (b) pushing of colluvium and initiation of undrained strength loss; (c) initiation of colluvial flow slide; (d) enlargement of colluvial flow slide

was delivered by the Phase I slide mass from the upper slope in 2014 (Fig. 9).

The fluidized material incorporated water ponded along the slope toe, as well as additional water that had accumulated in the colluvium since 2006. This allowed the colluvial mass to lose significant strength and flow to the slope toe and beyond, loading, liquefying, and entraining further quantities of water-filled colluvium and river alluvium. Fig. 10 shows that rafted blocks of unsaturated outwash sands and glacial till from the Whitman Bench traveled to near the alignment of SR530 (see line with small dashes). Conversely, the liquefied colluvium flowed over SR530 and continued for another 0.5 km past SR530 on the west side of the hill in Fig. 10.

Fig. 11 illustrates the mechanism of undrained strength loss in the disturbed colluvium by rapid loading and the resulting flowslide on Sassa (1985, 2000) and Hutchinson and Bhandari (1971). Sassa (1985) hypothesizes that shallow landslides from steep slopes may surcharge downslope loose granular soil so rapidly as to cause "impact liquefaction" (Fig. 11), a process he later duplicated in an undrained ring shear apparatus (Sassa 2000).

Fig. 12 is a view from SR530 showing the fluid nature of the colluvium, piles of rafted outwash sand from the Whitman Bench in the background, and some still upright trees that were carried on top of the rafted sand blocks from north of the river. This is evidence that the fluid colluvium moved farther than the outwash sands from the Whitman Bench (Phase 1), which was riding or rafting along on some of the liquefied colluvium. Fig. 12 also shows the fluid nature of the colluvium shortly after the flowslide and the more intact or frictional outwash sands and glacial till from the Whitman Bench in the background. In particular, the colluvial

Fig. 12. View of colluvial flow slide from SR530 with some tress still standing on top of a rafted sand block from the Phase I slide mass in the middle distance

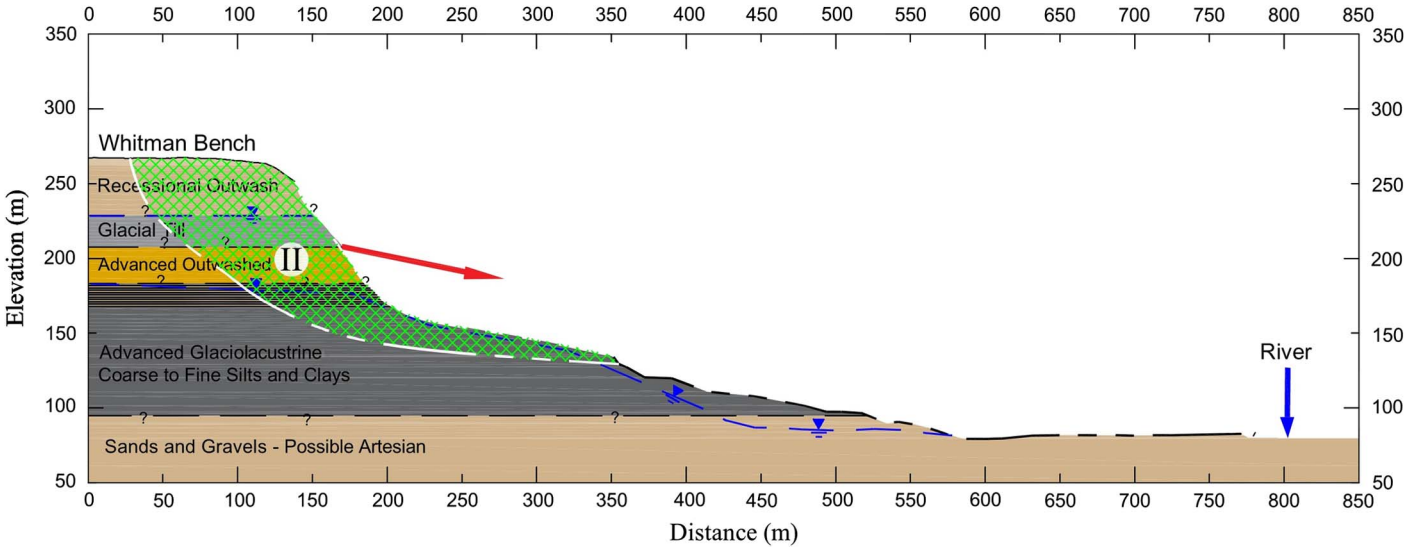

Fig. 13. Phase II failure surface–based field observations and inverse slope stability analyses at cross section location shown in Fig. 1

deposit shows little structure in front of the Phase I slide mass, whereas Fig. 12 shows significant deposits of sand, some of which still had trees in a vertical to near-vertical position even after moving down the slope and part way across the valley. The rheology of the disturbed colluvium (fluidlike) is clearly different from the rheology of the Phase I initial slide mass, which involved unsaturated materials, e.g., outwash sands and glacial till, and remained frictional instead of exhibiting fluid or liquefied behavior.

Phase II of Failure Mechanism: Whitman Bench Slide Mass

The mobility of the colluvium and Phase I initial slide mass caused unbuttressing of the upper slope, which initiated a retrogression into the intact material of the Whitman Bench. Based on inverse limit equilibrium stability analyses, Fig. 13 shows the probable compound failure surface for the Phase II slide mass that primarily involved the upper portion of the slope. The Phase II slide mass involves mostly unsaturated and intact outwash sands, glacial till, and the upper portion of the advanced glaciolacustrine clay deposit. The unsaturated portions of outwash and till deposits exhibited frictional behavior, which resulted in the formation of large landslide blocks instead of a flowslide as observed in the colluvium. As a result, the Phase II slide mass was much less mobile and is not responsible for any of the property damage or loss of life in the valley. The top of this slide mass forms the new landslide bench (Fig. 10) that will protect the overlying Whitman Bench for many years to come because the river cannot directly erode this bench or the upper plateau due to the lower portion of the Phase II slide mass covering the lower portion of the slope.

Fig. 14 shows an aerial photograph of the slope in July 2013, which shows the location of the 2006 headscarp and the extent of the Phases I and II slide masses in 2014. The Phase II slide mass primarily involves the Whitman Bench, while the Phase 1 slide mass involves part of the Whitman Bench and the slope below the 2006 headscarp. The Phase II slide mass also involves the mature trees that were located on the Whitman Bench prior to the 2014 landslide and are now on the new landslide bench shown in Fig. 10.

Aerial photographs show the Whitman Bench slope remained stable for more than 100 years and LiDAR images of adjacent slopes show similar slopes have remained stable for much longer. However, landslides involving the lower portion of the slope will continue to occur as the river erodes the 2014 landslide debris and undermines portions of the new and still tree-covered landslide bench (arrow in Fig. 10), but these lower-elevation slides will not directly impact the Whitman Bench. Based on river erosion rates calculated for the 1937, 1951, 1952, 1967, 1988, and 2006 landslides, it will take at least 300 years to remove enough of the Phase II slide mass and landslide bench to oversteepen and/or undermine the Whitman Bench sufficiently to cause another large landslide that moves past the river and across the valley as in 2014. This is an estimate because of differences in the ancient and 2014 landslide benches and differences in river erosion rates from 1937 to 2006 and after 2014, so the time for another large landslide to occur may increase or decrease. As a result, studying the effect of the river on the new landslide bench using LiDAR images, as shown in Fig. 7, is important to evaluate the landslide hazard and risk with time as discussed subsequently.

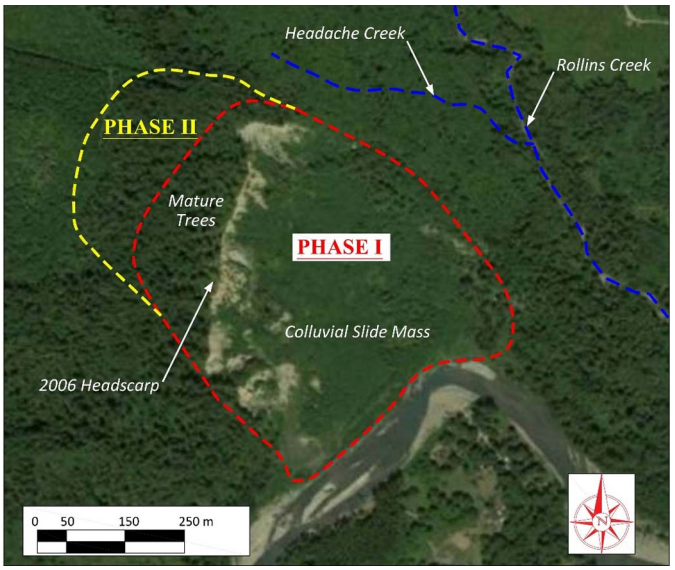

Fig. 14. Aerial view of slope in July 2013 and outline of the 2014 Phases I and II slide masses (© 2014 Google)

Identifying areas where the river has caused significant reduction in the existing landslide bench using LiDAR images is important and can explain the different return periods of the landslides that have occurred in this valley. The difference in these times is the level of erosion these slide masses underwent after their occurrence, which can be determined from LiDAR images. As a result, LiDAR imaging is important to improving landslide hazard assessments and guiding land use policies in similar valleys more so than dating prior landslides.

A time of 300 years is also in agreement with LiDAR interpretations presented by Haugerud (2014), which shows that 15 large landslides have occurred in this portion of the Stillaguamish River Valley over the last 6,000 years. This corresponds to a large landslide approximately every 400 years. This is an average return period for areas where the Stillaguamish River is actively eroding the slope toe and causing low-elevation landslides. LaHausen et al. (2015) used radiocarbon dating and numerical landscape modeling to refine the time estimate by Haugerud (2014) of 6,000 years and show that other large slides in this valley occurred between 500 and 5,000 years ago.

Fig. 10 shows that the Phase II slide mass stretched or spread out as it moved down the slope but did not become highly mobile like the colluvial flowslide. The runout of the Phase II slide mass was limited because it was mainly frictional and its leading edge collided with the back edge of the Phase I slide mass. On the western end, the Phase II slide mass actually overrode the northern edge of the Phase I slide mass because some advanced glaciolacustrine clay from the Phase II slide mass was found overlying the outwash sands of the Phase I slide mass (dashed circle in Fig. 10).

Seismic Records

The two-phase failure mechanism described previously is also in agreement with nearby seismograph recordings that show two distinct ground motions separated by approximately 2 min. The first ground motion recording started at 10:37.30 a.m. on March 22, 2014, and ended at 10:40.00 a.m., while the second motion started at 10:42.00 a.m. and lasted only 1.5 min. Hibert et al. (2014) also conclude these ground motions correspond to two separate landslide events (Phase I and II) with the events having different characteristics and runouts. The first motion is indicative of mobilization and acceleration of a large landslide mass with a velocity and acceleration of 19.4 m/s and 1.0 m/s^2 (Hibert et al. 2014). This first motion caused the colluvial flow slide, while the second motion is more impulsive and indicative of a complex breakaway sequence that merged into one landslide (Hibert et al. 2014), which reflects the retrogressive Phase II slide mass. Because of the fluid nature of the colluvial flowslide, a separate motion was not detected for this movement.

In summary, Fig. 9 summarizes the two large slope movements involved in the two-phase failure mechanism, which was initially described in a 1 June 2015 *Seattle Times* newspaper article (Doughton 2015). The Phase I slide mass moved first with significant speed and momentum, as described by an eyewitness (described subsequently), and impacted the colluvium that had accumulated on the lower part of the slope. The Phase I slide mass impacted, pushed, and overrode the water-filled colluvium in front of it and caused the colluvial flow slide that moved rapidly across the river and the valley, entombed the unexpecting neighborhood, SR530 highway, and beyond. The steep valley slope then remained unsupported and some 2 min later the Phase II slide mass slid down the cleared slope but did not move far because the materials were primarily unsaturated, dense, and frictional so it stopped at the back edge of the Phase I slide mass.

This is in agreement with the specific recollections from various eyewitnesses from Keaton et al. (2014) that reinforce the proposed two-phase failure mechanism (Fig. 9) and the seismic recordings:

- Observation that "half" of the upper portion of the slope, i.e., source zone, initially "broke away" and surged toward the Stillaguamish River;
- Reported period of relative quiescence between an initial stage (Phase I) of landsliding (estimated to be 1.5 min by an eyewitness) and a later mass movement (Phase II);
- Rapid inundation by a tall ("above roof lines of homes"), fast-moving, and highly liquid debris flow mass, e.g., debris was a "thick river of mud";
- Eyewitness reports that when the landslide hit the river, it accelerated;
- Soft and "quicksandlike" condition of the saturated debris flow deposits immediately following the landslide. "The water (in the debris field) was only maybe two inches deep, but the ground was so saturated my leg went all the way down to my knee"; and
- Douglas firs falling and breaking; and
- Splash marks high up in some pre-existing trees.

Unlike other large landslides, such as La Conchita, videos of the slide are not available so the proposed failure mechanism may not represent all aspects of the failure mechanism. For example, the geometry of the Phase I slide mass is subjective because the slide mass and scarp were removed. The Phase I slide mass geometry was estimated using results of inverse analyses of the 1967 and 2006 landslides to estimate groundwater and shear strength conditions that were used to predict the critical compound failure surface shown in Fig. 9.

Review of Other Failure Mechanisms

Keaton et al. (2014) present a deep-seated circular failure mechanism that extends to the slope toe and river. This failure mechanism is not plausible because it does not explain many field observations including:

- Presence of an override zone in Fig. 10;
- Absence of a back-tilted, largely intact slide block that is typical for deep-seated rotational sliding;
- Pervasive internal distortion and shearing of the Phase II slide deposits, and probably also the Phase I deposits, which were subsequently covered by Phase II and/or part of Phase I;
- Outwash sands being displaced to near SR530 with many trees at or near vertical;
- Big scalloplike slides in the Phase II slide mass;
- Some pre-existing trees still standing near vertical in the valley indicating a fluid slide mass;
- Nonhomogeneous and anisotropic slope stratigraphy, which results in a compound, not circular, failure surface;
- Splash marks high up in some pre-existing trees; and
- A deep-seated failure cannot push the colluvium along the slope toe a distance of 1.5 km.

Keaton et al. (2014) revised their failure mechanism from the deep-seated circular failure mechanism to a similar two-phase failure mechanism as presented herein (Wartman et al. 2016). The two-phase failure mechanism presented herein was presented at various professional meetings in April 2015 and published in the *Seattle Times* on June 1, 2015 (Doughton 2015). However, Wartman et al. (2016) still use circular failure surfaces in their new two-phase failure mechanism instead of compound failure surfaces to reflect the nonhomogeneous and anisotropic materials as suggested herein.

George and Iverson (2014), Iverson and George (2014, 2015), and Iverson et al. (2016) conclude that the failure mechanism

involves a lower portion of the slope moving and displacing the colluvium along the slope toe and some of the underlying, bedded sediments. This movement purportedly caused liquefaction of the water-saturated cohesionless sediment underlying the colluvium. This liquefaction is attributed to compression and/or shear-induced sediment contraction caused by a landslide in the lower segment of the slope that withdrew support from the slope above. In other words, the landslide started at a low elevation and progressed upward instead of starting at or above the ancient landslide bench and riding down the slope onto the water-filled colluvium as proposed herein. Such a mechanism would require the bulk of the advanced glaciolacustrine and glaciofluvial materials and even the glacial till to be either highly sensitive or liquefiable. This is inconsistent with the material properties presented herein.

Tart (2016) has a similar two-phase failure mechanism as presented herein but it initiates on the west side of the Ancient Landslide Bench instead of the east side where the bench width has been reduced significantly by the river erosion–induced landslides. Tart (2016) hypothesizes that a shallow circular slide occurred in the ancient landslide bench and on the west side fell into the 0.9–1.2 km^2 (15–20 acres) sedimentation pond constructed after the 2006 landslide (described previously), creating a large splash zone.

Liquefaction of Colluvium and Precedent

This section discusses the colluvial flowslide that was triggered by the Phase I slide mass impacting the water-filled, softened, and disturbed colluvium and causing a rapid undrained loading and large undrained strength loss. The term *liquefaction* is usually used to describe a large strength loss in saturated cohesionless soils subjected to rapid loading, such as an earthquake (Kramer 2004). However, the term has also been used to describe a soil or soil mass undergoing a large strength loss and phase change from a solid to a liquid without a change in density in other situations. This includes conditions in which the extreme loss of soil strength and rigidity occurs under static, undrained conditions, i.e., without earthquake shaking. For example, Casagrande (1940) reports liquefaction in loose deposits of hydraulically placed sand without a seismic event. Terzaghi (1957) and Bjerrum (1971) describe liquefaction of loose deltaic sand deposits under water. Morgenstern (1992) describes "spontaneous" liquefaction as the collapse of a loose, unstable granular soil skeleton when overstressed in shear. In summary, a range of natural and artificial soils can undergo a phase change and the conditions under which this can occur is wider than just a loose, saturated cohesionless soil subjected to an earthquake (Hunter and Fell 2003a, b).

For this paper, the relevant questions are whether or not some types of colluvium (soil disturbed by prior slope movement) can liquefy and is there precedent for the 2014 colluvial flow slide that entombed the Steelhead Haven community. The size and runout of the 2014 landslide had not been experienced in recent times at this location so precedence for the 2014 landslide was sought using local and global landslide data. Haugerud (2014) and LaHausen et al. (2015) use LiDAR images of the Stillaguamish River Valley to show that many large landslides involving the Whitman Bench have occurred over the last 5,000–6,000 years near the 2014 landslide. The 2014 landslide has similar shape and runout as these prior landslides based on interpretation of LiDAR images. Haugerud (2014) even shows that the 2014 landslide is not the largest prior landslide in this area of the Stillaguamish River Valley in the last 6,000 years (see the Rowan Landslide in Fig. 8).

Using a slide volume of 8.3 million m^3 and a ratio of landslide height (H) to travel distance (L) of approximately 0.1, the 2014 landslide plots near the lower bound of the database of prior large landslides in Hunter and Fell (2003a) but above the majority of the flowslides studied. Landslide height is the vertical distance measured from the top of the scarp to the end of the runout and the travel distance is the horizontal distance measured from the scarp to the toe of the runout deposit as defined by Hunter and Fell (2003a). Based on LiDAR images and the database of large landslides assembled by Hunter and Fell (2003a), the 2014 landslide is not an outlier, which is not surprising given that the H/L ratio for the slope is only 0.1.

A more relevant precedence than landslide size or H/L ratio is whether or not a heavily overconsolidated glacial clay has ever experienced a large runout as the 2014 landslide. A case history that has many similarities to the 2014 landslide is the 1973 Attachie landslide on the Peace River near Ft. St. John in British Columbia, Canada (Fletcher et al. 2002). Sliding occurred in a thick and complex sequence of heavily overconsolidated glaciolacustrine clays that was covered by approximately 30 m (100 ft) of glacial till, which is similar to the 2014 landslide stratigraphy with the advanced glaciolacustrine deposits being covered by outwash sands and glacial till deposits. The glaciolacustrine soil, forming the most mobile part of the Attachie landslide, consists of overconsolidated low-plasticity silt and plastic clayey silt with a liquidity index less than 0.3, all of which are similar to the advanced glaciolacustrine deposit involved in the 2014 landslide (Table 1). The 1973 Attachie landslide involved 7.5 million m^3 of silt, clay, and glacial till–derived colluvium created by previous landslides with limited mobility. The 1973 landslide also followed wet weather and crossed a 1-km-wide river channel in seconds, raising a displacement wave against the opposite bank. Fletcher et al. (2002) hypothesize that the high mobility was caused by spontaneous liquefaction of the loose silt matrix, redeposited around blocks of the overconsolidated original glacial till that was broken up by prior landslides. A similar change in shear behavior was observed at La Conchita, California, in 2005, where an extremely rapid, deadly flowslide was formed from silty colluvium from a slow earthflow 10 years earlier in 1995 (Jibson 2005). However, the 2005 La Conchita landslide differs from the 2014 Oso landslide because eyewitnesses claim the landslide started at the slope toe not near the top of the slope.

In summary, this paper uses the term *liquefaction* in a wider sense, as suggested by Hungr et al. (2014), to describe the rapid undrained loading and undrained strength loss in the water-filled, softened, and disturbed colluvium along the slope toe even though it does not involve loose, saturated sand subjected to an earthquake. This rapid undrained loading and strength loss in the water-filled colluvium is depicted in Fig. 11 and resulted in the colluvial flowslide that covered the Steelhead Haven community.

Landslide Hazard Mappings

Understanding the failure mechanism for the 2014 landslide is important for guiding future landslide hazard mapping using LiDAR images, which was expanded by the state legislature after the 2014 landslide. LiDAR images should be used to identify the following two slope configurations that can result in a high-elevation landslide and a large runout:

1. Areas where the entire slope, i.e., slope toe to upper plateau, has been oversteepened and/or undermined by prior sliding, river erosion, and/or other activity so it exhibits a steep and high slope, such as the Rowan landslide (LaHausen et al. 2015); and
2. Areas that are not steep over the entire slope length because of a significant accumulation of colluvium along the slope toe and

do not exhibit a wide ancient landslide bench to support the upper plateau, such as the 2014 Oso Landslide.

Both of these areas should be identified as high risk because the upper portion of the slope has high potential energy that can push the downslope deposits into and possibly across the valley instead of stopping at or near the river as the low-elevation landslides do. An example of the first high-risk area is the Rowan landslide that is located just west of the 2014 landslide (Fig. 8) and occurred 2,000–5,000 years ago (LaHausen et al. 2015). This landslide was caused by the Stillaguamish River oversteepening the entire slope, i.e., from the river to the upper plateau, so there was no flat area along the slope toe or significant ancient landslide bench before the landslide. The Rowan landslide is even larger than the 2014 landslide (Haugerud 2014) so LiDAR images should be studied to identify areas where the entire slope is oversteepened and/or undermined by prior sliding, river erosion, and/or other activity.

An example of the second high-risk area is the 2014 landslide where the slope was not as steep as the Rowan landslide slope but resulted in a similar runout. The 2014 landslide slope was not as steep because a significant colluvial deposit had accumulated along the slope toe, which reduced the overall slope inclination. However, the ancient landslide bench at this location was not sufficiently wide and/or the advanced glaciolacustrine deposit was not sufficiently strong enough to support the upper plateau or Whitman Bench. This set the stage for the Phase I initial slide mass to impact the water filled colluvium and cause the colluvial flowslide. Therefore, slope height alone is not a good risk indicator because many other slopes along this valley have a similar or greater slope height (LiDAR in Fig. 8) but the ancient landslide bench supporting the upper plateau in those slopes has not been compromised as it was on the eastern end of the 2014 landslide area and the lower portion of the slope is not filled with disturbed and water-filled colluvium that can undergo a significant undrained strength loss.

If the ancient landslide bench is still sufficiently wide and the advanced glaciolacustrine deposit is sufficiently strong to support the upper plateau, only landslides in the lower portion of the slope will occur, which will impact the river as in 1937, 1951, 1952, 1967, 1988, and 2006, and not the majority of the valley. This explains why even landslides that initiate at the same or higher elevation than the 2014 landslide do not always runout across the valley because the ancient landslide bench is able to support the upper plateau.

Summary

This paper summarizes the investigation, testing, analysis, and slope history used to determine the two-phase failure mechanism of the March 22, 2014, landslide near Oso, Washington, that destroyed more than 40 homes and fatally injured 43 people. The key findings are:

- The 2014 landslide occurred in two phases. Phase I consists of an initial landslide involving the upper plateau, i.e., Whitman Bench, that was oversteepened by the 2006 landslide. Phase II is a retrogressive landslide in the upper terrace caused by evacuation of the Phase I slide mass, which left the upper plateau unbuttressed.
- Rainfall in the 21 days before the 2014 landslide is the highest on record and corresponds to a 97-year return period, which contributed to initiation of the Phase I landslide on the eastern end of the ancient landslide bench.
- The Phase I landslide impacted, pushed, and overrode the water-filled, disturbed, and softened colluvium along the slope toe, causing a dramatic undrained strength loss (liquefaction) that enabled the colluvium to flow approximately 1.5 km across the valley.
- Phase II did not exhibit a large runout because the materials are dense, unsaturated, frictional, and were stopped by the back of the Phase I slide mass.
- The size and runout of the 2014 landslide are not unprecedented for similar ratios of slope height to runout distance in this valley and other locations (Hunter and Fell 2003a).
- Future LiDAR hazard mapping should identify the following two areas because they pose a high risk of a large runout across the valley floor: (1) slopes that have been oversteepened and/or undermined by prior sliding, river erosion, and/or other activity, e.g., the Rowan landslide in Fig. 8, and (2) areas that are not steep over the entire slope length because of a significant accumulation of colluvium along the slope toe but do not exhibit an ancient landslide bench sufficiently wide to support the upper plateau, e.g., the 2014 landslide. Therefore, slope height alone is not a good indicator because many other slopes along the valley have a similar or greater height than the 2014 landslide but have a slope profile, i.e., the Ancient Landslide Bench, that is sufficient to maintain adequate stability of the upper plateau.

Acknowledgments

The contents and views in this paper are those of the individual authors and do not necessarily reflect those of any of the represented corporations, agencies, organizations, and/or contributors. The authors acknowledge the information, site access, and samples provided by Snohomish County, information provided by the Washington Department of Transportation (WSDOT), and the financial support provided by the Department of Civil and Environmental Engineering at the University of Illinois at Urbana-Champaign. This support is gratefully acknowledged. It is also acknowledged that Oldrich Hungr is participating in some of the litigation matters related to the landslide.

References

ASTM. (2007). "Standard test method for particle-size analysis of soils." *ASTM D422*, West Conshohocken, PA.

ASTM. (2010a). "Standard test method for liquid limit, plastic limit, and plasticity index of soils." *ASTM D4318*, West Conshohocken, PA.

ASTM. (2010b). "Standard test method for torsional ring shear test to determine drained fully softened shear strength and nonlinear strength envelope of cohesive soils (using normally consolidated specimen) for slopes with no preesixting shear surfaces." *ASTM D7608*, West Conshohocken, PA.

ASTM. (2011). "Standard test method for one-dimensional consolidation properties of soils using incremental loading." *ASTM D2435*, West Conshohocken, PA.

ASTM. (2013). "Standard test method for torsional ring shear test to determine drained residual shear strength of cohesive soils." *ASTM D6467*, West Conshohocken, PA.

ASTM. (2015). "New test method for pocket penetrometer." *ASTM WK27337*, West Conshohocken, PA.

ASTM. (2016). "Standard test methods for laboratory miniature vane shear test for saturated fine-grained clayey soil." *ASTM D4648*, West Conshohocken, PA.

Badger, T. C. (2015). "Geotechnical report: SR 520 MP 35 to 41 geotechnical study, Washington." Washington Dept. of Transportation, Olympia, WA.

Bjerrum, L. (1971). "Subaqueous slope failures in Norwegian fjords." *Proc., 1st Int. Conf. on Port and Ocean Engineering under Arctic Conditions*, Vol. 1, Norwegian Geotechnical, Oslo, Norway, 24–47.

Cao, Q., Henn, B., and Lettenmaier, D. P. (2014). "Analysis of local precipitation accumulation return periods preceding the 2014 Oso mudslide." Dept. of Civil and Environmental Engineering, Univ. of Washington, Seattle.

Casagrande, A. (1940). "Characteristics of cohesionless soils affecting the stability of slopes and earth fills." *Contributions to soil mechanics 1925 to 1940*, Boston Society of Civil Engineers, Boston, 257–276.

Doughton, S. (2015). "Laser map gave clue to Oso slide's ferocity." ⟨http://www.seattletimes.com/seattle-news/science/laser-map-gave-clue-to-oso-slides-ferocity/⟩ (Jun. 2, 2015).

Dragovich, J. D., Stanton, B. W., Lingley Jr, W. S., Griesel, G. A., and Polenz, M. (2003). "Geologic map of the mount Higgins 7.5-minute quadrangle, Skagit and Snohomish Counties, Washington." *Rep. No. 2003-12*, Washington Divisions of Geology and Earth Resources, Olympia, WA.

Fletcher, L., Hungr, O., and Evans, S. G. (2002). "Contrasting failure behaviour of two large landslides in clay and silt." *Can. Geotech. J.*, 39(1), 46–62.

Gamez, J., and Stark, T. D. (2014). "Fully softened shear strength at low stresses for levee and embankment design." *J. Geotech. Geoenviron. Eng.*, 10.1061/(ASCE)GT.1943-5606.0001151, 06014010.

George, D. L., and Iverson, R. M. (2014). "A depth-averaged debris-flow model that includes the effects of evolving dilatancy. II: Numerical predictions and experimental tests." *Proc. R. Soc. London: Math. Phys. Eng. Sci.*, 470(2170), 20130820.

Haugerud, R. A. (2014). "Preliminary interpretation of pre-2014 landslide deposits in the vicinity of Oso, Washington: U.S." *Rep. No. 2014–1065*, Geological Survey, Reston, VA.

Henn, B., et al. (2015). "Hydroclimatic conditions preceding the March 2014 Oso landslide." *J. Hydrometeorol.*, 16(3), 1243–1249.

Hibert, C., Stark, C. P., and Ekstrom, G. (2014). "Seismology of the Oso-Steelhead landslide." *Nat. Hazards Earth Syst. Sci. Discuss.*, 2(12), 7309–7327.

Holtz, R. D., Kovacs, W. D., and Sheahan, T. C. (2011). *Introduction to geotechnical engineering*, Prentice Hall, Englewood cliffs, NJ.

Hungr, O., Leroueil, S., and Picarelli, L. (2014). "The varnes classification of landslide types, an update." *Landslides*, 11(2), 167–194.

Hunter, G. J., and Fell, R. (2003a). "Mechanics of failure of soil slopes leading to" rapid" failure." *Fast slope movements: Prediction and prevention for risk mitigation*, L. Picarelli, ed., Patron Editore, Bologna, Italy, 283–290.

Hunter, G. J., and Fell, R. (2003b). "Travel distance angle for 'rapid' landslides in constructed and natural soil slopes." *Can. Geotech. J.*, 40(6), 1123–1141.

Hutchinson, J. N., and Bhandari, R. K. (1971). "Undrained loading, a fundamental mechanism of mudflows and other mass movements." *Geotechnique*, 21(4), 353–358.

Iverson, R. M., et al. (2015). "Landslide mobility and hazards: Implications of the 2014 Oso disaster." *Earth Planetary Sci. Lett.*, 412(1), 197–208.

Iverson, R. M., and George, D. L. (2014). "A depth-averaged debris-flow model that includes the effects of evolving dilatancy. I: Physical basis." *Proc. R. Soc. London A: Math. Phys. Eng. Sci.*, 470(2170), 20130819.

Iverson, R. M., and George, D. L. (2016). "Modelling landslide liquefaction, mobility bifurcation and the dynamics of the 2014 Oso disaster." *Géotechnique*, 66(3), 175–187.

Jibson, R. W. (2005). "Landslide hazards at La Conchita, California." *Rep. No. 2005–1067*, U.S. Geological Survey, Denver.

Keaton, J. R., et al. (2014). "The 22 March 2014 Oso Landslide, Snohomish County, Washington." Geotechnical Extreme Event Reconnaissance (GEER), National Science Foundation, Arlington, VA.

Kim, J. W., Lu, Z., Qu, F., and Hu, X. (2015). "Pre-2014 mudslides at Oso revealed by InSAR and multi-source DEM analysis." *Geomatics Nat. Hazards Risk*, 6(3), 184–194.

Kramer, S. L. (2004). *Geotechnical earthquake engineering*, Prentice Hall, Upper Saddle River, NJ.

LaHausen, S. R., Duvall, A. R., Booth, A. M., and Montgomery, D. R. (2015). "Surface roughness dating of long-runout landslides near Oso, Washington (USA), reveals persistent postglacial hillslope instability." *Geology*, 139(6), 853–862.

Morgenstern, N. R. (1992). "The evaluation of slope stability: A 25 year perspective." *Proc., Stability and Performance of Slopes and Embankments*, ASCE, Reston, VA, 1–26.

Peck, R. B., Hanson, W. E., and Thornburn, T. H. (1974). *Foundation engineering*, 2nd Ed., Wiley, Hoboken, NJ.

Sassa, K. (1985). "The mechanism of debris flow." *Proc., XI Int. Conf. on Soil Mechanics and Foundation Engineering (SMFE)*, Vol. 2, CRC Press, Taylor & Francis Group, Boca Raton, FL, 1173–1176.

Sassa, K. (2000). "Mechanism of flows in granular soils." *Proc., Int. Conf. of Geotechnical and Geological Engineering, GEOENG2000*, Vol. 1, Technomic Publishing, Lancaster, PA, 1671–1702.

Seattle Times. (2016). "Building toward disaster." ⟨http://projects.seattletimes.com/2014/building-toward-disaster/⟩ (Oct. 3, 2016).

Shannon, W. D. (1952). "Report on slide on north fork Stillaguamish River near Hazel." U.S. Dept. of Game and Fisheries, Washington, DC.

SLIDE [Computer software]. Rocscience, Toronto.

SLOPE/W [Computer software]. Geo-slope International, Calgary, AB, Canada.

Stark, T. D., and Hussain, M. (2013). "Drained shear strength correlations for slope stability analyses." *J. Geotech. Eng.*, 10.1061/(ASCE)GT.1943-5606.0000824, 853–862.

Sun, Q., Zhang, L., Ding, X., Hu, J., and Liang, H. (2015). "Investigation of slow-moving landslides from ALOS/PALSAR images with TCPInSAR: A case study of Oso, USA." *Remote Sens.*, 7(1), 72–88.

Tart, R. G. (2016). "Why the Oso landslide caused so much death and destruction." *Proc., 2016 Geotechnical and Structural Engineering Congress*, ASCE, Reston, VA , 1545–1554.

Terzaghi, K. (1957). "Varieties of submarine slope failures." *Harvard soil mechanics series*, Wiley and Sons, Hoboken, NJ.

Thorsen, G. W. (1969). "Landslide of January 1967 which diverted the north fork of the Stillaguamish River near Hazel." Dept. of Natural Resources, Geology and Earth Resources Division, Olympia, WA.

Wartman, J., et al. (2016). "The 22 March 2014 Oso landslide, Washington, USA." *J. Geomorphol.*, 253(1), 275–288.